Multiple-Load Induction Cooking Application with Three-Leg Inverter Configuration

P. Sharath Kumar[†], N. Vishwanathan[*], and Bhagwan K. Murthy[*]

[†,*]Department of Electrical Engineering, National Institute of Technology Warangal, Telangana, India

Abstract

Inverter configurations for multiple-load induction cooking applications need development. Inverter configurations for induction cooking applications are used in home appliances based on single coil inverters. For multiple-load configurations, multiple coils are used. They require proper inverters, which provide independent control for each load and have fewer components. This paper presents a three-leg inverter configuration for three load induction cooking applications. Each induction coil powers one induction cooking load. This configuration operates with constant switching frequency and powers individual loads. The output power of the required load is controlled with a phase-shift control technique. This configuration is simulated and experimentally tested with three induction loads. The simulation and experimental results are in good agreement. This configuration can be extended to more loads.

Key words: Induction cooking, Multiple-loads, Phase shift control

I. INTRODUCTION

Induction cooking is one of the applications of induction heating. Conventionally, heating of any object involves the transfer of heat from the heat source to the object heated by conduction or radiation. The method of induction heating involves the development of heat directly in the object heated. A high frequency alternating current flowing through a coil wound over the object induces eddy currents in it. These eddy currents result in I^2R losses in the object and result in heating. Fig. 1 shows the typical arrangement of a high frequency induction heating circuit.

A resonant inverter is commonly used as a source of high frequency AC supply. DC input is derived by rectifying the utility AC source. High frequency AC flowing in the load coil results in eddy currents induced in the vessel at skin depth level resulting in a heating effect. The heat generated by the eddy currents in the load is concentrated in a peripheral layer at skin depth (δ) [1], which is expressed as

$$\delta = \sqrt{\frac{\rho}{\pi \mu f_s}} = \sqrt{\frac{1}{4\pi^2 \times 10^{-7}}} \times \sqrt{\frac{\rho}{\mu_r f_s}} \qquad (1)$$

where, ρ is electrical resistivity, μ is magnetic permeability, μ_r is the relative magnetic permeability of the load material, and f_s is the switching frequency of the inverter.

The high frequency alternating current is induced by a high frequency inverter. The frequency of the alternating current is decided by the material of the heated vessel. The vessels may be composed of either magnetic or non-magnetic material. Based on this, the range of frequency for induction cooking is 20 kHz to 150 kHz. These are resonated with a capacitor because of the inherently low power factor of the induction-heating load. Hence, series resonant inverters are the common choice for high-frequency induction cooking systems. Commonly preferred configurations are quasi-resonant, half-bridge, and full-bridge resonant inverters [1]-[4], [19]. Half-bridge configuration is mostly preferred, whereas for high power applications, full-bridge configuration may be used. The control of the output power of these resonant inverters can be achieved through certain methods, such as pulse amplitude modulation (PAM), pulse frequency modulation (PFM), phase-shift (PS) control, asymmetric voltage cancellation (AVC), asymmetric duty cycle (ADC) control, and hybrid control technique [5]-[11], [25]. These control techniques have their relative merits and demerits.

Multiple-load induction cooking systems are in focus for suitable inverter configurations. The main function of
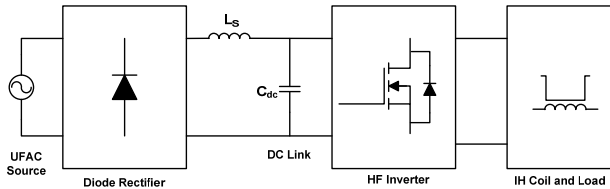
Fig. 1. Typical arrangement of an induction cooking resonant inverter.

Fig. 2. Three-leg inverter configuration.

inverters in multiple-load induction cooking systems is to reduce components count, simultaneous and independent control of each load, and high conversion efficiency. An inverter with two loads is proposed and analyzed in [12]. This method has one master and one slave load, and uses several resonant capacitors connected in parallel with electro-mechanical switches. The control of load power is achieved by activating these electro-mechanical switches. The disadvantages of this method are a large number of capacitors and use of electro-mechanical switches. An inverter configuration for two-loads is presented in [13], which has three legs (six switching devices). One leg of the inverter is common for both loads, and offers independent control of each load with high efficiency. It also offers a reduced component count and better device utilization. AVC control technique is adopted for power control. In [14], a two-output induction cooking system with power factor correction is proposed. Power control for each load is performed using the AVC control technique. In [15], a load-adaptive control algorithm is used for variable load and large output power range. Aspects such as efficiency, acoustic noise, and flicker control are considered in the design stage. For different ranges of output power, different control techniques are adopted. Though certain objectives are met, it makes the control structure more involved. To improve light-load performance, discontinuous conduction mode control is adopted in [16], and uses variable frequencies in the range 20kHz to 150kHz. It improves light load efficiency to 95%, but variable frequency operation is the limitation of this technique. The digital implementation of induction heating load is proposed in [17]. An AC-AC power conversion technique is presented in [18] for a multiple induction heating system. It has higher efficiency, a reduced components count, and reduced complexity, however uses variable frequency control, which is the limitation of this method.

In the above-mentioned literature for multiple-load application, either the inverters have a larger components count or variable frequency control is adopted. Enough scope exits in this area for further improvement with constant frequency control and reduced complexity. In this paper, a three-leg inverter configuration is presented for a three-load induction cooking system. It offers constant switching frequency operation, simple control, less components count, and high efficiency.
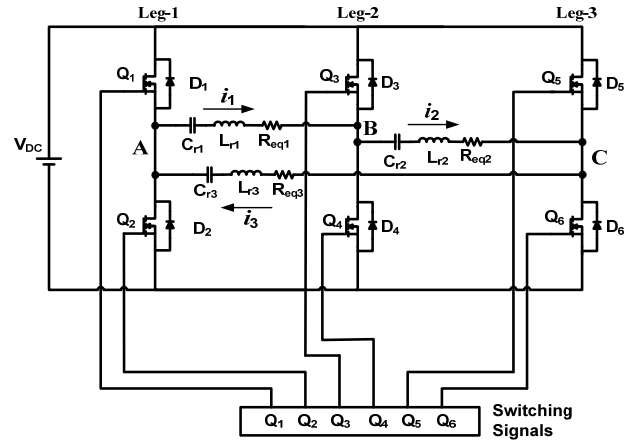
This paper is organized as follows. In Section II, principle of operation of three-leg inverter configuration is presented. Section III describes the simulation and experimental results. Section IV presents characteristics showing power control of loads. Section V presents extension of this configuration to more than three loads. Section VI concludes the paper.

II. THREE-LEG INVERTER CONFIGURATION AND CONTROL SCHEME

This section describes the inverter configuration and control scheme for a three-load induction cooking application. Fig. 2 shows the circuit diagram of this configuration. Fig. 3 shows only load resonant tank circuits, where three loads are connected in delta across inverter output voltages v_{AB}, v_{BC}, and v_{CA}.

An induction cooking system consists of a vessel and an induction coil. The coil and vessel are similar to the primary and secondary of a transformer. Based on this, induction cooking load in refferrence to the coil is modeled as a series R_{eq} - L_r circuit for constant switching frequency operation [12], [20]-[24]. R_{eq} is the referred equivalent resistance and L_r is the referred equivalent inductance to the coil, respectively.

The concept of series resonance is used with each load. The resonant load circuits are connected in delta at the output terminals of the inverter configuration. They are marked as leg-1, leg-2, and leg-3. Load-1 consists of C_{r1}, L_{r1}, and R_{eq1}, which are resonant capacitor, inductance of the load-1, and equivalent load resistance in series with resonant tank, respectively. For load-2, C_{r2}, L_{r2}, and R_{eq2} are the resonant capacitor, inductance of the load-2, and equivalent load resistance in series with resonant tank, respectively. Similarly for load-3, C_{r3}, L_{r3}, and R_{eq3} are the resonant capacitor, inductance of the load-3, and equivalent load resistance in series with resonant tank, respectively.

Under an equal maximum output power of all loads, the inverter is switched at 30kHz and the gate pulses of each leg are phase shifted by 120° w. r. t. other leg pulses. All
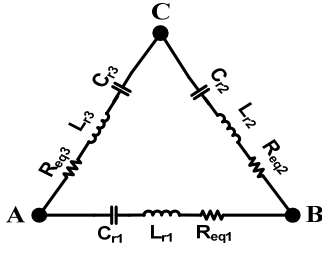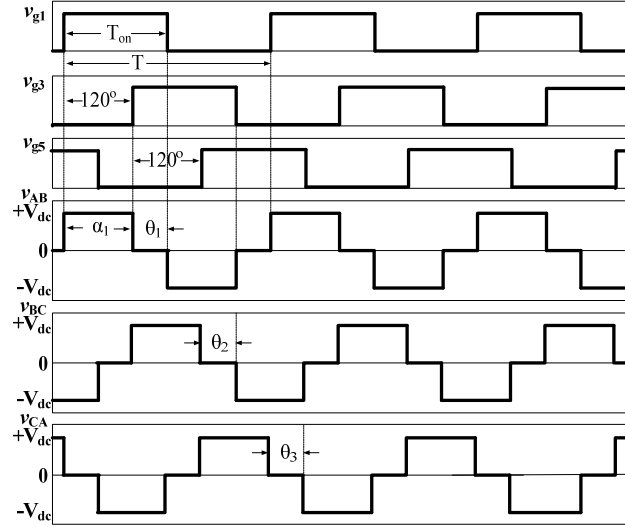
Fig. 3. Three load resonant circuit.

Fig. 4. Inverter gate pulses and output voltage waveforms v_{AB}, v_{BC}, and v_{CA}.

three-load circuits have the same component values and all inverter legs are operated at the same switching frequency. Hence, the resonant frequencies of all load circuits have to be the same. The resonant frequency of each load circuit is $f_r = \frac{1}{2\pi\sqrt{L_r C_r}}$. The switching frequency of each leg is slightly higher than their resonant frequency. The inverter switching frequency (f_s) is chosen at 5% to 10% higher than the resonant frequency (f_r) for ZVS operation.

In this configuration, the duty-ratio of the gate pulses is kept constant. Fig. 4 shows the gate pulses v_{g1}, v_{g3}, and v_{g5} for the switching devices Q_1, Q_3, and Q_5, respectively. These are 120° phase shifted with each other. The gate pulses of Q_2, Q_4, and Q_6 are 180° out of phase w.r.t. Q_1, Q_3, and Q_5 respectively. The inverter output voltages across loads are v_{AB}, v_{BC}, and v_{CA}.

An analysis of PS control of series resonant inverter is presented in [10]. Fig. 5 shows the inverter voltage waveform (v_{AB}) for the load-1 and load-1 current (i_1) of the three-leg inverter. v_{AB1} is the fundamental component of v_{AB}. The current in the resonant tank is close to sine wave because of the filtering of harmonics by the LC resonant tank. Harmonics in load current waveforms are negligible. I_1, I_2, and I_3 are the r.m.s values of the load currents.

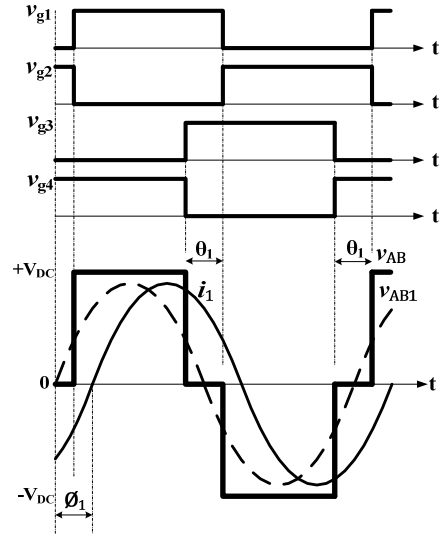In PS control, the peak value of v_{AB1} is expressed as:

Fig. 5. Output voltage and current with control variables.

$$\hat{v}_{AB1} = \frac{4V_{dc}}{\pi}\cos\frac{\theta_1}{2} \tag{2}$$

$\hat{I}_1$ is the peak amplitude of the load-1 current assumed sinusoidal, and $\emptyset_1$ is the power factor angle.

$$\hat{I}_1 = \frac{\hat{v}_{AB1}}{|Z_{eq}|}$$
$$= \frac{4V_{DC}}{\pi|Z_{eq}|}\cos\frac{\theta_1}{2}$$
$$= \frac{4V_{DC}\cos\emptyset_1}{\pi R_{eq}}\cos\frac{\theta_1}{2} \tag{3}$$

The output power of load-1 is expressed as:

$$P_{o1} = \frac{\hat{I}_1^2}{2}R_{eq1}$$
$$= \frac{8V_{DC}^2\cos^2\emptyset_1}{\pi^2 R_{eq1}}\cos^2\frac{\theta_1}{2} \tag{4}$$

P_{o2} and P_{o3} are output powers of load-2 and load-3, respectively. The total output power (P_T) is expressed as $P_T = P_{o1} + P_{o2} + P_{o3}$.

The quality factor (Q) for load-1 and normalized switching frequency (ω_n) are expressed as:

$$Q = \frac{\sqrt{\frac{L_{r1}}{C_{r1}}}}{R_{eq}} \tag{5}$$

$$\omega_n = \frac{\omega_s}{\omega_{r1}} \text{ and } \omega_{r1} = \frac{1}{\sqrt{L_{r1}C_{r1}}} \tag{6}$$

where ω_s is angular switching frequency and ω_r is the angular resonant frequency.

From the above equations, the amplitude of the fundamental component of output voltage can be controlled by varying θ. Consequently, the load current and output power also can be controlled by varying θ.

From Fig. 4,

$$\theta_1 = 180° - \alpha_1 \tag{7}$$

$$(240° + \theta_2) = (\alpha_1 + 180°) \tag{8}$$

$$\theta_2 = (\alpha_1 - 60°) = (120° - \theta_1) \tag{9}$$

From Eqs. (7) and (9),

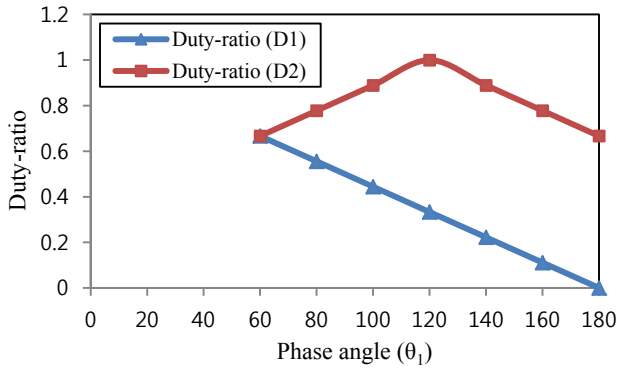$$D_1 = \frac{180° - |\theta_1|}{180°} \tag{10}$$

Fig. 6. Variation of duty-ratios vs. phase angle(θ_1).

$$D_2 = \frac{180^o - |\theta_2|}{180^o} \qquad (11)$$

Eqs. (7) to (11) show that D_1 and D_2 are dependent on θ_1 and θ_2, respectively. These are in turn dependent on α_1. Fig. 6 shows the variation of duty-ratios D_1 and D_2 w.r.t. phase angle(θ_1). As leg-2 is common for load-1 and load-2, the variation of D_1 results in the variation of D_2 in a certain manner, which is justified by Eq. (9). θ_3 will not be affected because load-3 is not connected to leg-2. Hence, D_3 will not change.

The output powers of load-1 to load-3 are proportional to $\cos^2 \frac{\theta_1}{2}$, $\cos^2 \frac{\theta_2}{2}$, and $\cos^2 \frac{\theta_3}{2}$, respectively. As $\frac{\theta_1}{2}$ varies from 30° to 90°, $\frac{\theta_2}{2}$ varies from 30° to 0° and back to 30°. Hence $\cos^2 \frac{\theta_1}{2}$ varies from 0.75 to 0 and $\cos^2 \frac{\theta_2}{2}$ varies from 0.75 to 1 and back to 0.75. Whereas, $\cos^2 \frac{\theta_3}{2}$ does not vary at all. Full range control of load-1 power results in a 25% variation in load-2 power and no variation in load-3 power. In cooking applications, precise temperature control may not be very essential. This maximum variation of 25% in one of the loads when a particular load is controlled may not be a significant drawback.

III. RESULTS OF THREE-LEG INVERTER CONFIGURATION

The three-leg inverter configuration with the PSC technique is simulated and is experimentally verified using the parameters shown in Table I.

Fig. 7 shows the experimental set-up of a three-leg inverter configuration. Fig. 7(a) shows the induction heating loads with a 3-leg inverter circuit. Fig. 7(b) shows a 3-leg inverter circuit with a pulse generator and a driver circuit. In the control circuit, two UC3875 ICs are used for six control pulses with phase shift control. Three IR2110 ICs are used as drivers. The implementation of the control circuit is simple without any logic gates. This configuration is designed and operated at a switching frequency of 30kHz.
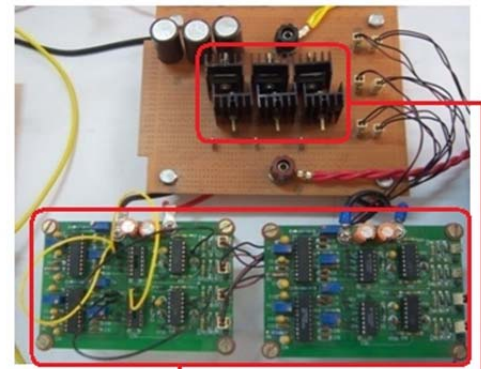
Fig. 8 shows the switching pulses for a 3-leg inverter configuration. Fig. 8(a) shows the switching pulses for upper

TABLE I
PARAMETERS OF THREE-LEG INVERTER CONFIGURATION

Item	Symbol	Value
Source voltage	V_{DC}	30 V
Equivalent resistance of each load	R_{eq}	1.95 Ω
Parasitic series resistance of IH each load coil		0.14 Ω
Equivalent inductance of each load	L_r	68 μH
Resonant capacitance of each load (EPCOS B25834-F6104-M001) [(3 x 0.1μF)+(0.15μF)=0.45μF]	C_r	0.45 μF
ESR for 0.15μF capacitor		24 mΩ
ESR for 0.1μF capacitor		33 mΩ
Delay time in each leg	t_d	450 nsec
Resonant frequency of load circuit	f_r	28.77 kHz
Switching frequency of each leg	f_s	30 kHz
MOSFETs used	IRFP4110PbF	100 V, 180 A
IRFP4110PbF - $R_{DS(on)}$		3.7 mΩ

Induction heating loads   **Resonant capacitors**

(a)

Control circuit   **3-leg inverter**

(b)

Fig. 7. Experimental set-up of the three-leg inverter configuration.
a   Induction heating loads with inverter circuit
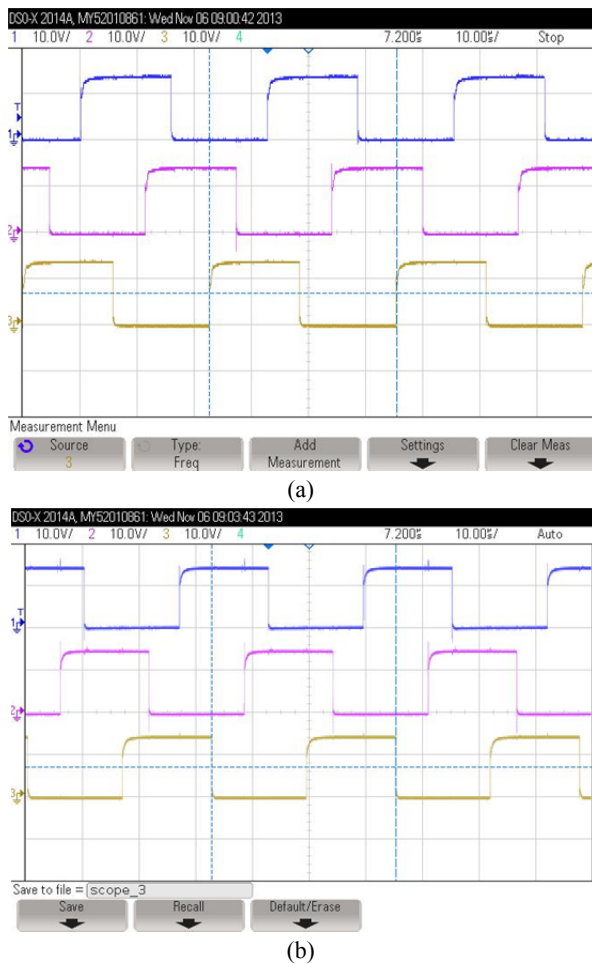b   3-leg inverter circuit with control circuit

Fig. 8. Switching pulses for a three-leg inverter.
a   Switching pulses for upper switching devices of each leg
b   Switching pulses for lower switching devices of each leg

switching devices Q_1, Q_3, and Q_5 of a 3-leg inverter. These pulses are 120° phase shifted with each other. Fig. 8(b) shows the switching pulses for lower switching devices Q_2, Q_4, and Q_6. These pulses are also 120° phase shifted with each other and 180° phase shifted with their respective upper switching device pulses.

All three loads are connected in delta. In addition, each load can be viewed as if connected to a full-bridge inverter. Each leg of the inverter is common for two loads. Under equal output power of all three loads, each output voltage is phase shifted from the other output voltage by 120º. Each load current is 120° phase shifted from one another. For the control of each load power θ_1, θ_2, and θ_3 can be controlled. Simulation and experimental results are shown in Figs. 9 to 10 for different PS combinations between leg-1 and leg-2. The load-1 current can be controlled by varying the phase angle (θ_1). Similarly, the load-2 current can be controlled by varying the phase angle (θ_2). For control of the load-3 current, phase angle (θ_3) is varied.

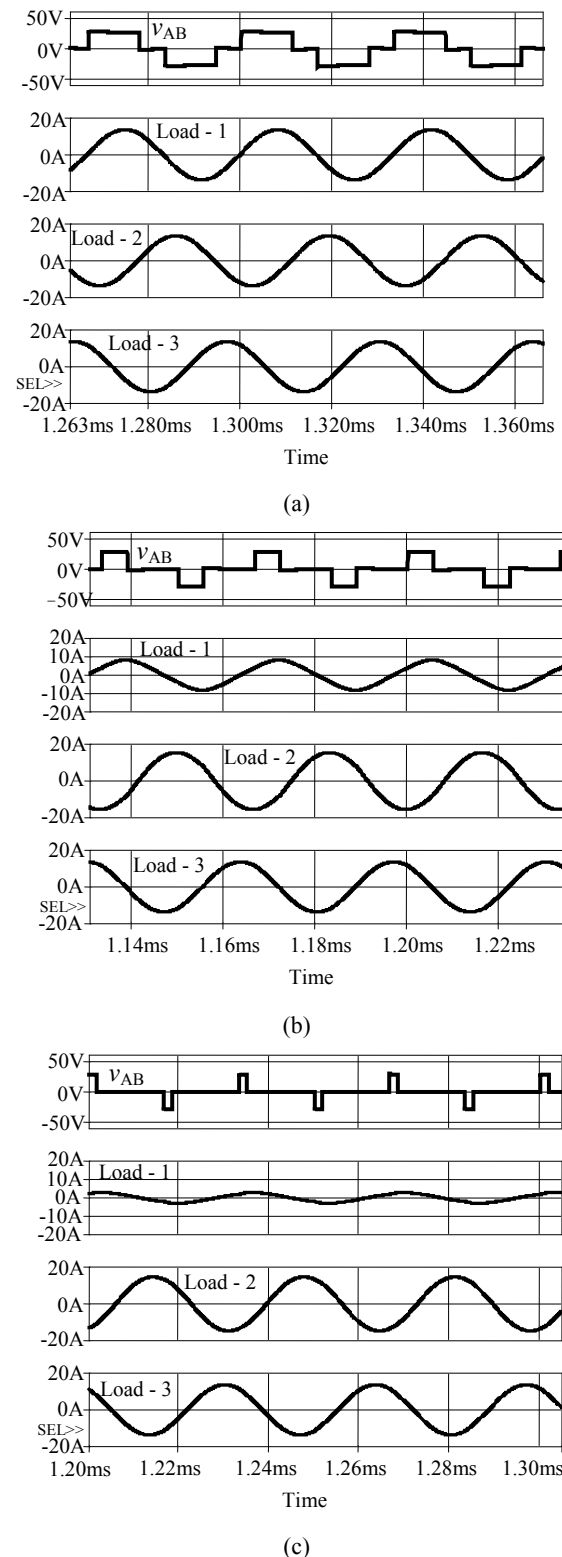Fig. 9 shows the simulation waveforms. Fig. 9(a) shows the inverter output voltage of load-1 and its load current
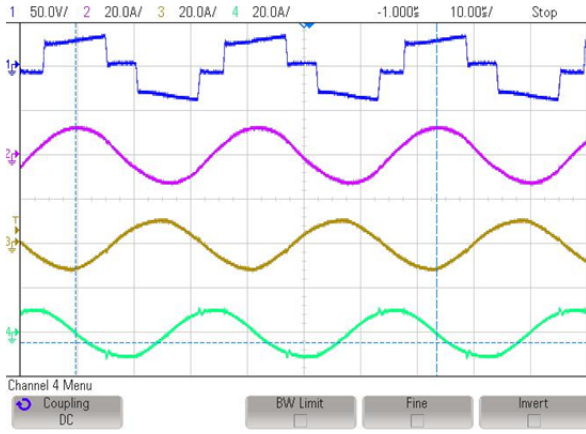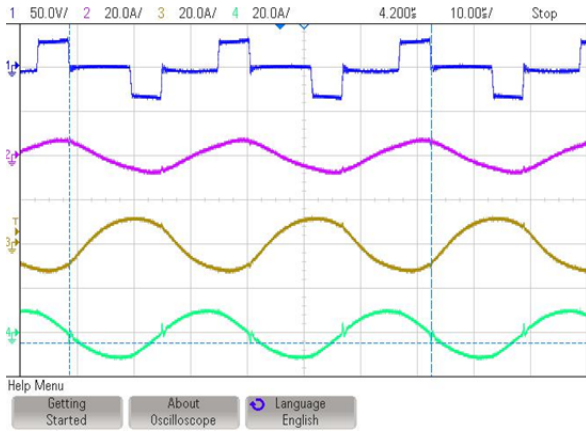

Fig. 9. Voltage waveform simulations across load-1 with all load currents.
a at $\theta_1 = 60°$; *b* at $\theta_1 = 120°$; *c* at $\theta_1 = 160°$

along with other two loads at $\theta_1 = 60°$. Fig. 9(b) shows these waveforms at $\theta_1 = 120°$. Fig. 9(c) shows these waveforms at $\theta_1 = 160°$.

(a)

(b)

(c)

Fig. 10. Experimental voltage waveforms across load-1 and all load currents.
a at $\theta_1 = 60°$; *b* at $\theta_1 = 120°$; *c* at $\theta_1 = 160°$

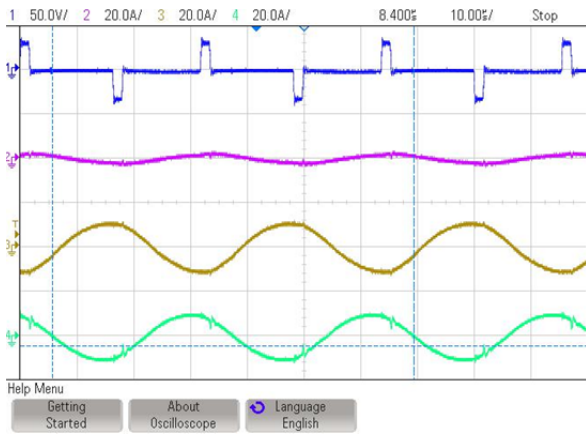Fig. 10 shows the experimental waveforms. Fig. 10(a) shows the inverter output voltage across load-1 and its load current along with other two loads at $\theta_1 = 60°$. Fig. 10(b) shows these waveforms at $\theta_1 = 120°$. Fig. 9(c) shows these waveforms at $\theta_1 = 160°$.

Both simulation and experimental results are in good agreement with each other. This configuration can power three loads simultaneously with constant switching
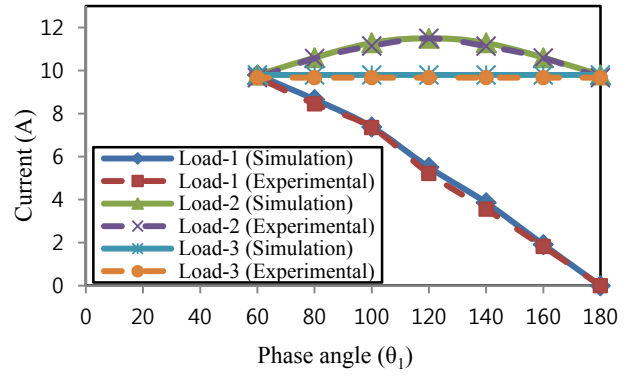

Fig. 11. Variation of load currents vs. phase angle (θ_1).

frequency.

In addition, any one-load current can be controlled using the PS control technique, which gives an almost independent power control of that load. In Figs. 9(a) to (c) and 10(a) to (c), the phase angle (θ_1) of load-1 is taken as 60°, 120° and 160°. Hence, the corresponding load-1 current is controlled by phase angle (θ_1). The current in load-2 varies because of the variation in θ_1, as shown in Fig. 11. With an increase in θ_1, the current in load-2 initially increases, reaching a peak, and then decreases. Hence, there is little variation in load-2 current when load-1 current is controlled. Load-3 current remains constant because its phase angle (θ_3) remains constant at 60°.

In induction cooking applications, this small variation of the load-2 current may be tolerable as precise temperature control is not required. This configuration gives the advantage of power control of the required load, and reduces components count and offers one leg / load.

Switching devices of 3-leg inverter configuration have ZVS at low phase angles(θ) with PS control technique; switching devices may not have ZVS at higher phase angles(θ), which is the limitation of this configuration.

IV. CONTROL OF LOAD POWER

In a 3-leg inverter configuration, required load power control can be achieved using the PS control technique. Each load power is dependent on corresponding load currents. Load currents are controlled with their phase angles(θ) and are experimentally verified. Load current magnitudes w.r.t. and their phase angles(θ) are shown in Table II.

The above table shows that when θ_1 varies, load-1 current is controlled. Load-2 current is slightly affected and load-3 current remains constant. The small variation of load-2 current may not be significant for cooking application. Similarly, the load-2 current can be controlled by varying θ_2 and the load-3 current can be controlled by varying θ_3. All load currents are in r.m.s. values under the experimental condition.

TABLE II
LOAD CURRENTS VS. ITS PHASE ANGLE (θ)

S. No	θ_1	Load-1 current	θ_2	Load-2 current	θ_3	Load-3 current
1	60°	9.673A	60°	9.673A	60°	9.673A
2	80°	8.449A	40°	10.567A	60°	9.673A
2	100°	7.491A	20°	11.147A	60°	9.673A
3	120°	5.216A	0°	11.5A	60°	9.673A
4	140°	3.55A	20°	11.135A	60°	9.673A
5	160°	1.821A	40°	10.585A	60°	9.673A
6	180°	0A	60°	9.673A	60°	9.673A
7	60°	9.673A	80°	8.449A	40°	10.567A
8	60°	9.673A	100°	7.491A	20°	11.147A
9	60°	9.673A	120°	5.216A	0°	11.5A
10	60°	9.673A	140°	3.55A	20°	11.135A
11	60°	9.673A	160°	1.821A	40°	10.585A
12	60°	9.673A	180°	0A	60°	9.673A
13	40°	10.567A	60°	9.673A	80°	8.449A
14	20°	11.147A	60°	9.673A	100°	7.491A
15	0°	11.5A	60°	9.673A	120°	5.216A
16	20°	11.135A	60°	9.673A	140°	3.55A
17	40°	10.585A	60°	9.673A	160°	1.821A
18	60°	9.673A	60°	9.673A	180°	0A

TABLE III
LOAD-1 OUTPUT POWER VS. ITS PHASE ANGLE (θ_1)

S. No	θ_1 (degree)	Output power (watts)
1	0°	257.89
2	20°	241.78
3	40°	218.48
4	60°	182.46
5	80°	139.2
6	100°	109.42
7	120°	53.05
8	140°	24.57
9	160°	6.47
10	180°	0

Fig. 11 shows load currents versus θ_1. For a variation of θ_1 from 60° to 180°, its load current varies from 9.673A to 0A. Under this condition, load-2 current has small variation, as leg-2 is common for load-1 and load-2. Under this variation of θ_1, θ_2 varies from 60° to 0° and back to 60°. However, θ_3 is remains constant at 60°. Each load current magnitude depends upon its load PS angle(θ). Simulation and experimental results are in good agreement with each other. Load-1 output power w.r.t. its phase angle(θ) is shown in Table III.

Fig. 12 shows the overall efficiency versus θ_1. Overall efficiency for this configuration is >93% for the entire control range of one load. Total output power is measured by adding the individual load outputs. Each load output is computed as $I^2 R_{eq}$. 'I' is the r.m.s. value of the respective load current. 'R_{eq}' is the equivalent load resistance of the respective load. Input power is obtained by multiplication of DC input voltage and average input current of the inverter.
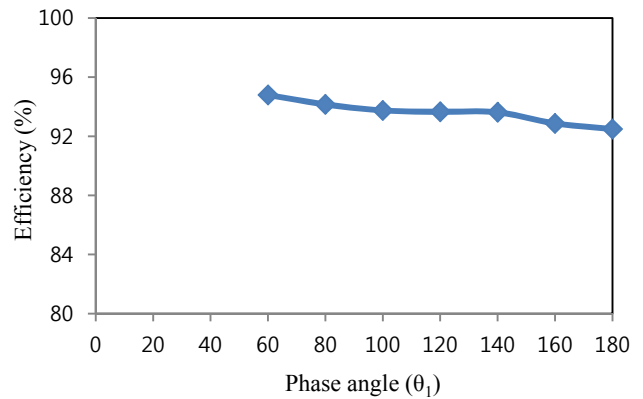

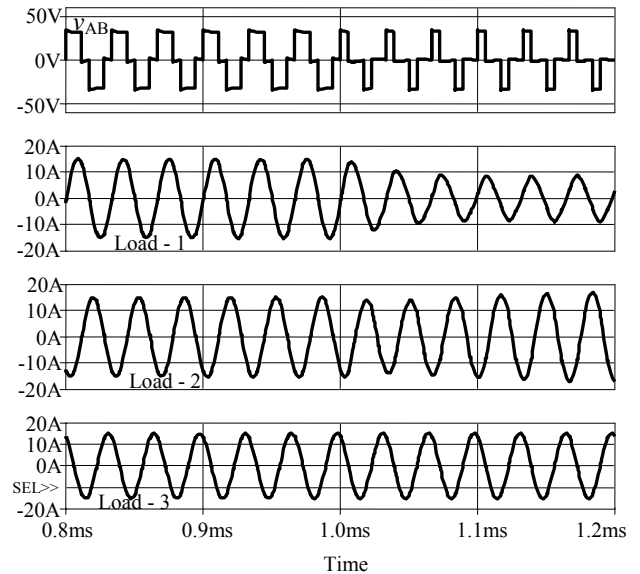Fig. 12. Overall efficiency vs. phase angle (θ_1).

Fig. 13. Transient variation of all load currents for sudden variation in D_1.

Fig. 13 shows the transient variation of all load currents for sudden variation in D_1 at 1 msec. Load-1 and load-2 currents have smooth transition to new steady state condition. Load-3 current is not affected.

From Eq. (7),

$$\theta_1 = 180° - \alpha_1$$
$$\text{Similarly, } \theta_2 = 180° - \alpha_2 \qquad (12)$$
$$\theta_3 = 180° - \alpha_3 \qquad (13)$$

α_1 and α_2 are controlled independently and α_3 is dependent on α_1 and α_2.

$$\alpha_3 = (\alpha_1 + \alpha_2) \qquad \text{up to } (\alpha_1 + \alpha_2) \leq 180° \qquad (14)$$
$$\alpha_3 = 360° - (\alpha_1 + \alpha_2) \qquad \text{for } (\alpha_1 + \alpha_2) > 180° \qquad (15)$$

Fig. 14 shows each load power control possibility in combination of all loads w.r.t. their α. In Fig. 14, X represents α_1 for load-1, Y represents α_2 for load-2, and Z represents α_3 for load-3. When α value is 0°, the load power is also zero. When α value changes from 0° to 180°, the load power changes from zero to maximum. Simultaneously, all loads can have equal maximum power for $\alpha_1 = \alpha_2 = \alpha_3 = 120°$ i.e., respective θ values are 60° each. For different combinations
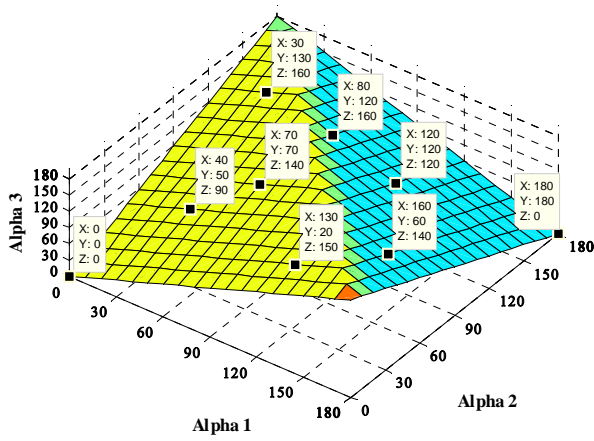
Fig. 14. Each load power control possibilities vs. their α.
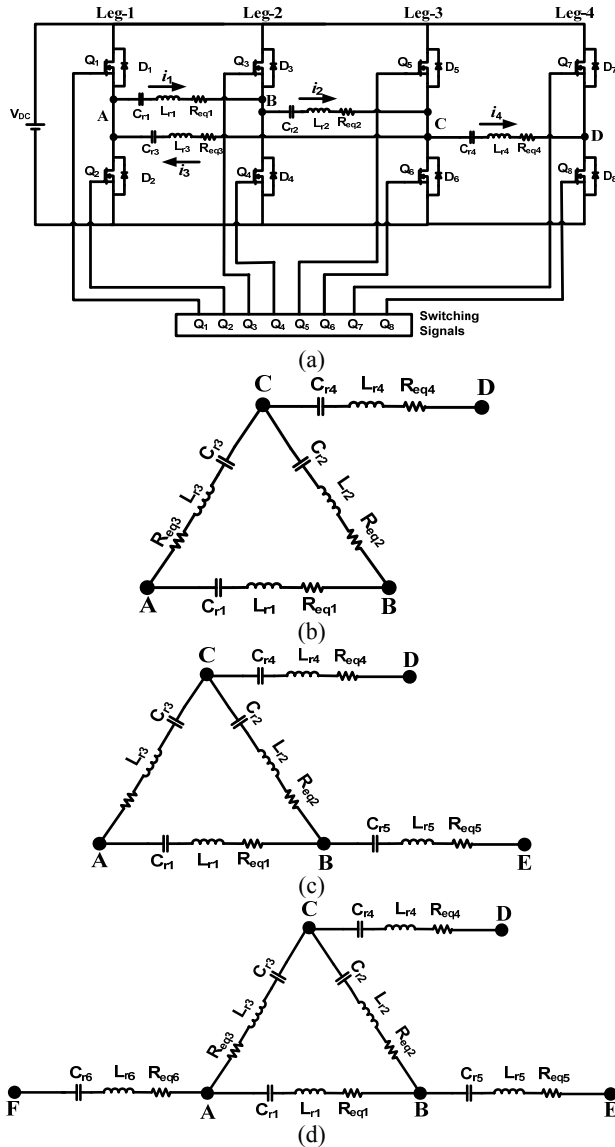

(a)

(b)

(c)

(d)

Fig. 15. Extension of the three-leg inverter configuration to multiple loads.
a Extension of three-leg inverter configuration to four-leg configuration;
b Four load resonant circuit*; c* Five load resonant circuit;
d Six load resonant circuit

of individual load powers, a look-up table can be made with possible values of α for wide operating flexibility.

V. EXTENSION OF THREE-LEG INVERTER CONFIGURATION

This configuration requires two switching devices per load or one leg per load, and is extended for multiple loads as shown in Fig. 15.

In Fig. 15(a), a three-leg configuration is extended for four loads by adding an additional leg to the right of leg-3. The switching frequency is same for the existing configuration. By controlling this load with the PS control technique, the load connected between leg-3 and this additional leg-4 can be independently controlled. Here also, the number of legs per load is one. Fig. 15(b) shows only load resonant circuits where three loads are connected in delta across the inverter output voltages v_{AB}, v_{BC}, and v_{CA}, respectively, and an addition of fourth load is across the inverter output voltage v_{CD}. Extension to fifth and sixth load is shown in Figs. 15(c) and (d) respectively. Independent control of fifth and sixth loads are possible with PS control technique. Hence, this method can be extended to six loads also with a number of legs per load equal to one.

VI. CONCLUSION

A three-leg inverter configuration with three loads for induction cooking applications has been presented. In this configuration, the required load can be controlled almost independently, and can be extended for more loads. The number of switching devices per load is two (i.e., one leg per load). Constant switching frequency is used for powering the loads. Each load is operated at a switching frequency of 30kHz. PS control technique is used for the power control of the required load. The design and output power control of this configuration is simple. This configuration can also be used for uniform surface heating with a minimum components count. The simulation and experimental results of this configuration are in good agreement.

REFERENCES

[1] S. M. W. Ahmed, M. M. Eissa, M. Edress, and T. S. Abdel-Hameed, "Experimental investigation of full bridge series resonant inverters for induction-heating cooking appliances," *4th IEEE Conference on Industrial Electronics and Applications,* ICIEA 2009, pp.3327-3332, 2009.

[2] M. Miyamae, T. Ito, K. Matsuse, and M. Tsukahara, "Performance of a high frequency quasi-resonant inverter with variable-frequency output for induction heating," *IEEE 7th International Power Electronics and Motion Control Conference*, 2012.

[3] A. Fujita, H. Sadakata, I. Hirota, H. Omori, and M. Nakaoka, "Latest developments of high-frequency series

load resonant inverter type built-in cooktops for induction heated all metallic appliances," *IPEMC'* 2009, pp. 2537-2544, 2009.

[4]   N. A. Ahmed and M. Nakaoka, "Boost-half-bridge edge resonant soft switching PWM high-frequency inverter for consumer induction heating appliances," *IEE Electric Power Applications*, Vol. 153, No. 6, pp. 932-938, Nov. 2006.

[5]   O. Jimenez, O. Lucia, I. Urriza, L. A. Barragan, and D. Navarro, "Design and evaluation of a low-cost high-performance $\Sigma - \Delta$ ADC for embedded control systems in induction heating appliances," *IEEE Trans. Ind. Electron.*, Vol. 61, No. 5, pp. 2601-2611, May 2014.

[6]   H. Sarnago, O. Lucia, A. Mediano, and J. M. Burdio, "Direct AC–AC resonant boost converter for efficient domestic induction heating applications," *IEEE Trans. Power Electron.*, Vol. 29, No. 3, pp. 1128-1139, Mar. 2014.

[7]   I. Millan, J. M. Burdío, J. Acero, O. Lucía, and S. Llorente, "Series resonant inverter with selective harmonic operation applied to all-metal domestic induction heating," *IET Trans. Power Electron.*, Vol. 4, No. 5, pp. 587-592, May 2011.

[8]   L. Meng, K. W. E. Cheng, and K. W. Chan, "Systematic approach to high-power and energy-efficient industrial induction cooker system: circuit design, control strategy, and prototype evaluation," *IEEE Trans. Power Electron.*, Vol. 26, No. 12, pp. 3754-3765, Dec. 2011.

[9]   J. Shen, H. Ma, W. Yan, J. Hui, and L. Wu, "PDM and PSM hybrid power control of a series-resonant inverter for induction heating applications," *IEEE Conference on Industrial Electronics and Applications (ICIEA)*, 2006.

[10] J. M. Burdio, L. A. Barragan, F. Monterde, D. Navarro, and J. Acero, "Asymmetrical voltage cancellation control for full-bridge series resonant inverters," *IEEE Trans. Power Electronics*, Vol. 19, No. 2, pp. 461-469, Mar. 2004.

[11] H. Sarnago, O. Lucia, A. Mediano, and J. M. Burdio, "Class D/DE dual-mode operation resonant converter for improved efficiency domestic induction heating system," *IEEE Trans. Power Electron.*, Vol. 28, No. 3, pp. 1274-1285, Mar. 2013.

[12] F. Forest, E. Laboure, F. Costa, and J. Y. Gaspard, "Principle of a multi-load / single converter system for low power induction heating," *IEEE Trans. Power Electron.*, Vol. 15, No. 2, pp. 223-230, Mar. 2000.

[13] J. M. Burdio, F. Monterde, J. R. Garcia, L. A. Barragan, and A. Martinez, "A two-output series-resonant inverter for induction-heating cooking appliances," *IEEE Trans. Power Electron.*, Vol. 20, No. 4, pp. 815-822, Jul. 2005.

[14] S. Zenitani, M. Okamoto, E. Hiraki, and T. Tanaka, "A charge boost type multi output full bridge high frequency soft switching inverter for IH cooking appliance," *14th International Power Electronics and Motion Control Conference (EPE-PEMC)*, pp. T2-127 - T2-133, 2010.

[15] O. Lucia, J. M. Burdio, I. Millan, J. Acero, D. Puyal, "Load-adaptive control algorithm of half-bridge series resonant inverter for domestic induction heating," *IEEE Trans. Ind. Electron.*, Vol. 56, No. 8, pp. 3106-3116, Aug. 2009.

[16] O. Lucia, J. M. Burdio, L. A. Barragan, C. Carretero, and J. Acero, "Series resonant multi-inverter with discontinuous-mode control for improved light-load operation," *IEEE Trans. Ind. Electron.*, Vol. 58, No. 11, pp. 5163-5171, Nov. 2011.

[17] O. Lucia, I. Urriza, Luis A. Barragan, D. Navarro, O. Jimenez, and J. M. Burdio, "Real time FPGA-based hardware in the loop simulation test bench applied to multiple output power converters," *IEEE Trans. Ind. Appl.*, Vol. 47, No. 2, pp. 853-860, Mar./Apr. 2011.

[18] O. Lucia, C. Carretero, J. M. Burdio, J. Acero, and F. Almazan, "Multiple-output resonant matrix converter for multiple induction heaters," *IEEE Trans. Ind. Appl.*, Vol. 48, No. 4, pp. 1387-1396, Jul./Aug. 2012.

[19] I. Sheikhian, N. Kaminski, S. Vob, W. Scholz, and E. Herweg, "Optimisation of the reverse conducting IGBT for zero-voltage switching applications such as induction cookers," *IET Trans. Circuits, Devices & Syst.*, Vol. 8, No. 3, pp. 176-181, May 2014.

[20] V. M. Primiani, S. Kovyryalov, and G. Cerri, "Rigorous electromagnetic model of an induction cooking system," *IET Trans. Science, Meas. & Technol.*, Vol. 6, No. 4, pp. 238-246, Jul. 2012.

[21] C. Carretero, O. Lucia, J. Acero, R. Alonso, and J. M. Burdio, "Frequency-dependent modelling of domestic induction heating systems using numerical methods for accurate time-domain simulation," *IET Trans. Power Electron.*, Vol. 5, No. 8, pp. 1291-1297, Sep. 2012.

[22] L. C. Meng, K. W. E. Cheng, K. W. Chan, and Y. Lu, "Variable turn pitch coils design for heating performance enhancement of commercial induction cooker," *IET Trans. Power Electron.*, Vol. 5, No. 1, pp. 134-141, Jan. 2012.

[23] J. Acero, C. Carretero, R. Alonso, and J. M. Burdio, "Quantitative evaluation of induction efficiency in domestic induction heating applications," *IEEE Trans. Magn.*, Vol. 49, No. 4, pp. 1382-1389, Apr. 2013.

[24] J. Acero, C. Carretero, I. Millan, O. Lucia, R. Alonso, and J. M. Burdio, "Analysis and modeling of planar concentric windings forming adaptable-diameter burners for induction heating appliances," *IEEE Trans. Power Electron.*, Vol. 26, No. 5, pp. 1546-1558, May 2011.

[25] O. Jimenez, O. Lucia, I. Urriza, L. A. Barragan, P. Mattavelli, and D. Boroyevich, "An FPGA-based gain-scheduled controller for resonant converters applied to induction cooktops," *IEEE Trans. Power Electron.*, Vol. 29, No. 4, pp. 2143-2152, Apr. 2014.

P. Sharath Kumar received a B.Tech degree in Electrical and Electronics Engineering from Jawaharlal Nehru Technological University, Hyderabad, India in 2006 and a M.Tech degree from the National Institute of Technology, Kurukshetra, India in 2008. He is presently pursuing a Ph.D. in Electrical Engineering at the National Institute of Technology, Warangal, India. His area of interest is high frequency resonant inverters for induction cooking and LED lighting applications.

N. Vishwanathan received a B.Sc (Engg.) degree in electrical engineering from Dayalbagh Educational Institute, Agra, India, in 1990, a M.Tech. degree in electrical machines and industrial drives from REC, Warangal, India in 1992, and a Ph.D. from Indian Institute of Science, Bangalore, India, in 2004. He is currently working as a Professor in the Dept. of Electrical Engg., NIT, Warangal, India. His areas of interest are switched mode power conversion and induction heating applications.

Bhagwan K. Murthy obtained his B.E. (Electrical) and M.E. (Industrial Electronics) degrees from the M. S. University of Baroda, India in 1983 and 1987, respectively. He did his Ph.D. at IIT Madras in 1999. He is working as Professor of Electrical Engineering at the National Institute of Technology, Warangal, India. His research interests include application of power electronics to DSP controlled industrial drives and renewable energy.